

μ SR Investigation and Suppression of T_C by overdoped Li in Diluted Ferromagnetic Semiconductor $\text{Li}_{1+y}(\text{Zn}_{1-x}\text{Mn}_x)\text{P}$

Huiyuan Man¹, Xin Gong¹, Guoxiang Zhi¹, Shengli Guo¹, Cui Ding¹, Quan Wang¹, T. Goko^{2,3}, L. Liu², B. A. Frandsen², Y. J. Uemura², H. Luetkens³, E. Morenzoni³, C.Q. Jin⁴, T. Munsie⁵, G.M. Luke^{5,6}, Hangdong Wang⁷, Bin Chen⁷ and F. L. Ning^{1*}

¹Department of Physics, Zhejiang University, Hangzhou 310027, China

²Department of Physics, Columbia University, New York, New York 10027, USA

³Paul Scherrer Institute, Laboratory for Muon Spin Spectroscopy, CH-5232 Villigen PSI, Switzerland

⁴Beijing National Laboratory for Condensed Matter Physics,

and Institute of Physics, Chinese Academy of Sciences, Beijing 100190, China

⁵Department of Physics and Astronomy, McMaster University, Hamilton, Ontario L8S4M1, Canada

⁶Canadian Institute for Advanced Research, Toronto, Ontario M5G1Z8, Canada and

⁷Department of Physics, Hangzhou Normal University, Hangzhou 310016, China

(Dated: January 25, 2022)

We use muon spin relaxation (μ SR) to investigate the magnetic properties of a bulk form diluted ferromagnetic semiconductor (DFS) $\text{Li}_{1.15}(\text{Zn}_{0.9}\text{Mn}_{0.1})\text{P}$ with $T_C \sim 22$ K. μ SR results confirm the gradual development of ferromagnetic ordering below T_C with a nearly 100% magnetic ordered volume. Despite its low carrier density, the relation between static internal field and Curie temperature observed for $\text{Li}(\text{Zn},\text{Mn})\text{P}$ is consistent with the trend found in $(\text{Ga},\text{Mn})\text{As}$ and other bulk DFSs, indicating these systems share a common mechanism for the ferromagnetic exchange interaction. $\text{Li}_{1+y}(\text{Zn}_{1-x}\text{Mn}_x)\text{P}$ has the advantage of decoupled carrier and spin doping, where Mn^{2+} substitution for Zn^{2+} introduces spins and Li^+ off-stoichiometry provides carriers. This advantage enables us to investigate the influence of overdoped Li on the ferromagnetic ordered state. Overdoping Li suppresses both T_C and saturation moments for a certain amount of spins, which indicates that more carriers are detrimental to the ferromagnetic exchange interaction, and that a delicate balance between charge and spin densities is required to achieve highest T_C .

PACS numbers: 75.50.Pp, 71.55.Ht, 76.75.+i

I. INTRODUCTION

The successful fabrication of III-V $(\text{In},\text{Mn})\text{As}$ and $(\text{Ga},\text{Mn})\text{As}$ through low temperature molecular beam epitaxy (LT-MBE) has generated extensive research into diluted ferromagnetic semiconductors (DFS).¹⁻⁸ Theoretically, it has been proposed that T_C can reach room temperature with sufficient spin and carrier density.⁹ After almost two decades' efforts, the Curie temperature T_C of $(\text{Ga},\text{Mn})\text{As}$ thin films has been improved to as high as 200 K.¹⁰⁻¹² One of the major intrinsic difficulties is the low solid solubility of Mn^{2+} substitution for Ga^{3+} , which makes it difficult to enhance the concentration of Mn while controlling the homogeneity of thin films. Mn^{2+} substitution for Ga^{3+} provides not only local moments but also hole carriers. During the fabrication of thin films, some Mn^{2+} easily get into the interstitial sites and become a double donor, which makes it difficult to determine precisely the amount of Mn that substitutes for Ga at the ionic sites.⁸ Investigating some DFS systems with more controllable spin and carrier density might be helpful in understanding the general mechanism of ferromagnetism.

Recently, several bulk form DFS families that are derivatives of FeAs-based high temperature superconductors have been reported.¹³⁻²² Among them, the T_C of 122 type bulk form $(\text{Ba},\text{K})(\text{Zn},\text{Mn})_2\text{As}_2$ reaches $\sim 180\text{K}$,²⁰ which is already comparable with

the record T_C of $(\text{GaMn})\text{As}$.^{11,12} μ SR measurements have shown that the relation between static internal field and Curie temperature observed in I-II-V $\text{Li}(\text{Zn},\text{Mn})\text{As}$,¹³ 1111 type $(\text{La},\text{Ba})(\text{Zn},\text{Mn})\text{AsO}$ ¹⁶ and 122 type $(\text{Ba},\text{K})(\text{Zn},\text{Mn})_2\text{As}_2$ ²⁰ DFSs all fall into the scaling observed in $(\text{Ga},\text{Mn})\text{As}$ thin films,²³ indicating they all share a common mechanism for the ferromagnetic exchange interaction. The availability of a specimen in bulk form also enables the NMR measurements of DFS. Through ⁷Li NMR of $\text{Li}(\text{Zn},\text{Mn})\text{P}$,¹⁴ Ding *et al.* successfully identified Li(Mn) sites that have Mn^{2+} at N.N. (nearest neighbor) sites, and found that the spin lattice relaxation rate $\frac{1}{T_1}$ is temperature independent above T_C , i.e., $\frac{1}{T_1} \sim 400 \text{ s}^{-1}$, indicating that Mn spin-spin interaction extends over many unit cells with an interaction energy $|J| \sim 100 \text{ K}$.²⁴ This explains why DFS exhibits a relatively high T_C with such a low density of Mn.

The other advantage of these new bulk DFSs is the decoupling of carrier and spin doping. $(\text{La},\text{Ba})(\text{Zn},\text{Mn})\text{AsO}$ DFS with $T_C \sim 40 \text{ K}$,¹⁶ for example, is achieved by doping Mn^{2+} and Ba^{2+} into the direct gap semiconductor LaZnAsO , where Mn^{2+} substitution for Zn^{2+} and Ba^{2+} substitution for La^{3+} introduce spin and hole carriers, respectively. Both Mn and Ba are chemically stable elements, and the concentrations of charge and spin can be precisely controlled. Very recently, by controlling the Li concentration and by doping Mn into the direct gap semiconductor LiZnP (gap $\sim 2.1 \text{ eV}$),^{25,26} $\text{Li}(\text{Zn},\text{Mn})\text{P}$ ¹⁴ has

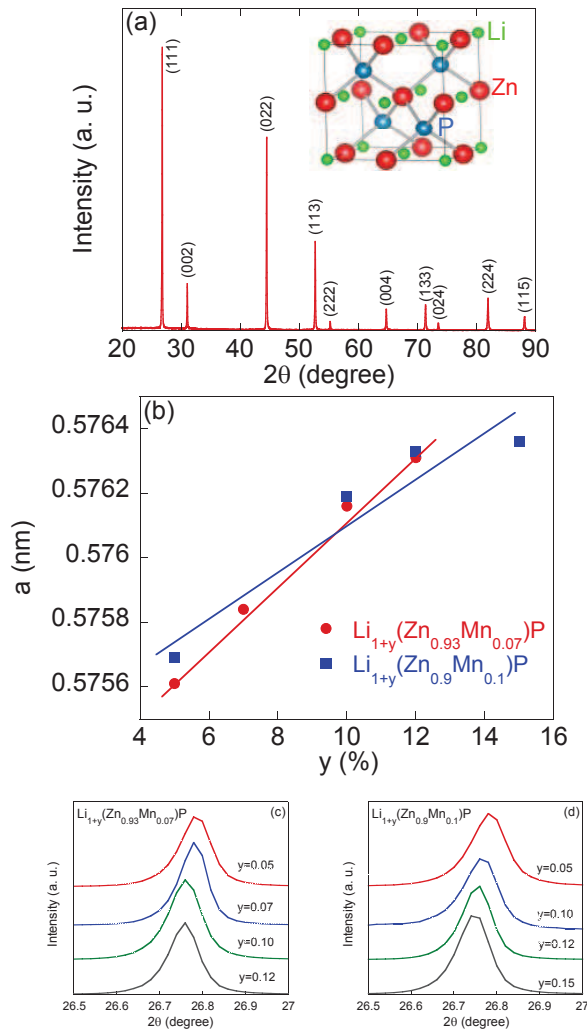


FIG. 1: (Color online) (a) Powder x-ray diffraction patterns of the parent compound LiZnP with the Miller indices. The inset shows the cubic lattice of LiZnP. (b) The lattice constants of $\text{Li}_{1+y}(\text{Zn}_{0.93}\text{Mn}_{0.07})\text{P}$ and $\text{Li}_{1+y}(\text{Zn}_{0.9}\text{Mn}_{0.1})\text{P}$, solid lines are guides for the eye. (c) and (d) Amplified plot of (111) peak for $\text{Li}_{1+y}(\text{Zn}_{0.93}\text{Mn}_{0.07})\text{P}$ and $\text{Li}_{1+y}(\text{Zn}_{0.9}\text{Mn}_{0.1})\text{P}$.

been found to experience a transition into ferromagnetic state below $\sim 34\text{K}$ with a low carrier density of $10^{16}/\text{cm}^3$. This carrier density is ~ 3 orders smaller than that of $(\text{Ga},\text{Mn})\text{As}$, $\text{Li}(\text{Zn},\text{Mn})\text{As}$ and $(\text{Ba},\text{K})(\text{Zn},\text{Mn})_2\text{As}_2$, leaving the open questions about the mechanism behind ferromagnetism of $\text{Li}(\text{Zn},\text{Mn})\text{P}$.

In this paper, we use μSR to investigate the ferromagnetism of a I-II-V DFS $\text{Li}(\text{Zn},\text{Mn})\text{P}$ with $T_C = 22\text{K}$. Our μSR results demonstrate that a nearly 100% ferromagnetic ordered volume develops below T_C , indicating the homogenous distribution of Mn^{2+} atoms. This result is consistent with NMR measurements of the same specimen. We also investigated the spin dynamics of Mn spins, and found that $\text{Li}(\text{Zn},\text{Mn})\text{P}$ also falls into the same scalings of internal field and T_C observed for $(\text{Ga},\text{Mn})\text{As}$

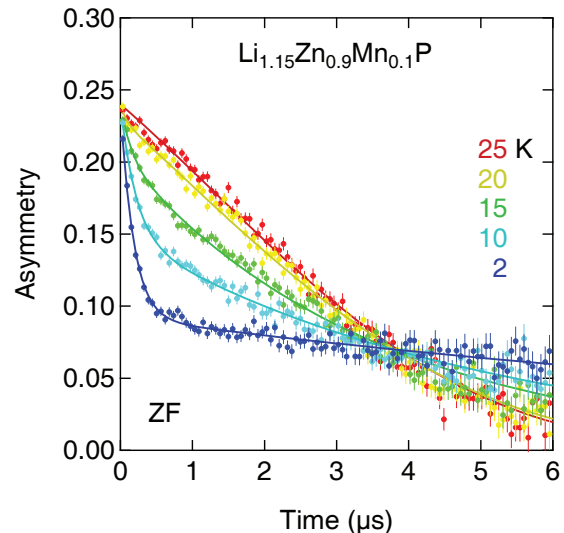


FIG. 2: (Color online) Time spectra of zero field μSR measurements for $\text{Li}_{1.15}\text{Zn}_{0.9}\text{Mn}_{0.1}\text{P}$ with $T_C \sim 22\text{K}$. The solid lines are fits to a two component relaxation function for dilute spin systems.¹³

and other bulk DFSs, indicating that $\text{Li}(\text{Zn},\text{Mn})\text{P}$ belongs to the DFS families that share a common mechanism of ferromagnetic exchange interaction despite its much lower carrier density. Furthermore, taking advantage of decoupled carrier and spin doping, we studied the carrier doping effect on the ferromagnetic ordered state. Our experimental results show that overdoping Li suppresses both T_C and the saturation moments. In other words, too many carriers are harmful to the development of ferromagnetic ordering in a similar way as too few.

II. EXPERIMENTS

The $\text{Li}_{1+y}(\text{Zn}_{1-x}\text{Mn}_x)\text{P}$ polycrystalline specimens were synthesized by the solid state reaction method. High purity elements of Li (99.9%), Zn (99.9%), Mn (99.99%), and P (99%) were mixed and slowly heated to 450°C in evacuated silica tubes, and held at 450°C for 48 hours. After cooling down to room temperature, the mixture was ground thoroughly, then pressed into pellets and heated again to ensure the complete reaction. The handling of materials was performed in a high-purity argon filled glove box (the percentage of O_2 and H_2O was ≤ 0.1 ppm) to protect it from air. Powder X-ray diffraction was performed at room temperature using a PANalytical X-ray diffractometer (Model EMPYREAN) with monochromatic $\text{CuK}\alpha_1$ radiation. The dc magnetization measurements were conducted on Quantum Design SQUID (superconducting quantum interference device). Zero-field (ZF) and weak-transverse-field (WTF) muon spin relaxation measurements were performed at PSI and TRIUMF. The specimen used for μSR study in this work is the same piece as used in the NMR study.²⁴

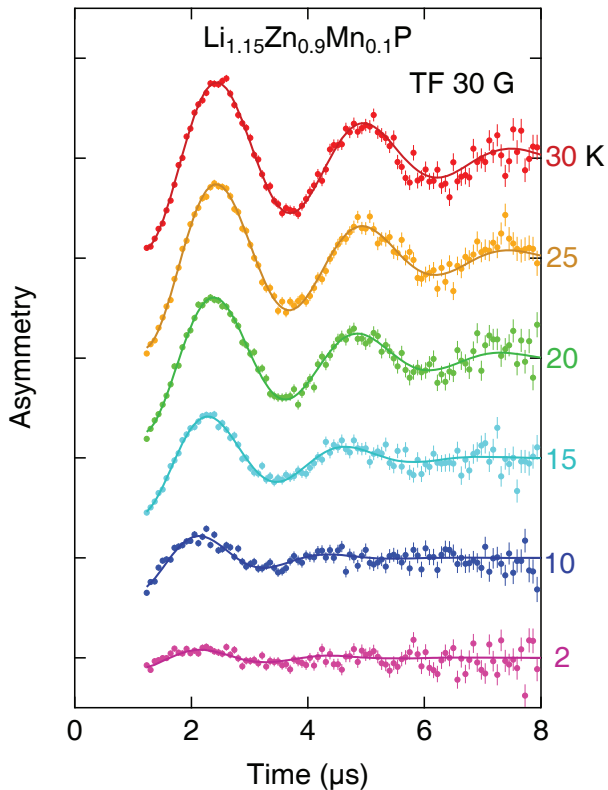


FIG. 3: (Color online) μ SR time spectra of $\text{Li}_{1.15}(\text{Zn}_{0.9}\text{Mn}_{0.1})\text{P}$ in a weak-transverse-field of 30 Oe. The oscillation amplitude corresponds to the paramagnetic volume fraction.

III. RESULTS AND DISCUSSION

In Fig 1(a), we show powder X-ray diffraction patterns of the parent compound LiZnP with the Miller indices. Bragg peaks can be well indexed into a cubic structure with a space group $F\bar{4}3m$, identical to the zinc blende GaAs .^{13,14} Doping excess Li and Mn into the parent compound does not change the crystal structure and no impurities have been observed. The lattice constants a of $\text{Li}_{1+y}(\text{Zn}_{0.93}\text{Mn}_{0.07})\text{P}$ and $\text{Li}_{1+y}(\text{Zn}_{0.9}\text{Mn}_{0.1})\text{P}$ are shown in Fig. 1(b). The evolution of lattice constant a follows the Vegard law, indicating the successful Li doping. This trend can also be seen from the amplified (111) peaks shown in Fig. 1(c) and (d), which shift systematically towards smaller 2θ with increasing y , suggesting that Li atoms are indeed incorporated into the lattice. This results in the enlargement of the unit cell. In addition, it has been shown that the NMR line width of LiZnP is only ~ 4 KHz.²⁴ This is comparable to the line width of pure Cu metal, indicating the high quality of these polycrystals. We do not observe signals arising from Li atoms that enter Zn sites which would give rise to additional NMR peaks due to the different electrical environment they are located in.²⁴

In Fig. 2, we show the time spectra of the

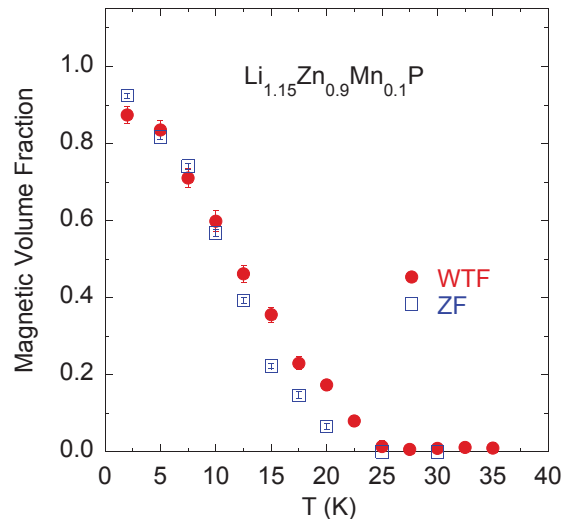


FIG. 4: (Color online) Temperature dependent magnetic volume fraction derived from ZF (\square) and WTF- μ SR (\bullet) measurements for $\text{Li}_{1.15}(\text{Zn}_{0.9}\text{Mn}_{0.1})\text{P}$.

Zero-field (ZF) μ SR on the polycrystalline sample $\text{Li}_{1.15}(\text{Zn}_{0.9}\text{Mn}_{0.1})\text{P}$ which has a $T_C = 22$ K. It can be seen that the time spectra clearly displays an increase in relaxation rate below $T = 15$ K. We note that no clear oscillation is observed even at 2 K; a similar situation is observed in $(\text{Ga},\text{Mn})\text{As}$ ²³ and $\text{Li}(\text{Zn},\text{Mn})\text{As}$ ¹³ as well. This can be attributed to the random distribution of Mn moments in real space because Mn substitution for Zn is random. This makes the local field at the muon site highly random even in the ferromagnetic ground state, and ZF precession signals are subsequently strongly damped. The random distribution of Mn moments has also been shown by $\text{Li}(\text{Mn})$ NMR lineshapes, which displays a large distribution between 61 MHz and 66 MHz.²⁴ The broad NMR line arises from the distribution of hyperfine fields at $\text{Li}(\text{Mn})$ sites, which can be as large as ~ 0.3 Tesla.²⁴ Note that the transferred hyperfine coupling between Li nuclear spins and Mn electrons is much weaker than those between Zn/Mn and As. Currently, we do not know the exact muon sites in $\text{Li}(\text{Zn},\text{Mn})\text{P}$, but relatively large hyperfine fields at muon sites are likely. We employed a two component function to analyze the ZF spectra (the fitting function is identical to the one used for $\text{Li}(\text{Zn},\text{Mn})\text{As}$, as explained in the method section of ref. 13). One component is for a static magnetic field with a Lorentzian distribution. This is expected for dilute Mn moments randomly substituting Zn sites, representing the magnetically ordered volume. The other component is an exponential function, representing the volume fraction of fluctuating paramagnetism. The derived ferromagnetic ordered volume fraction is shown in Fig. 4.

In Fig. 3, we show the μ SR time spectra measured in a weak transverse field (WTF) of 30 Oe. As stated

TABLE I: Curie temperature (T_C), Weiss temperature (θ), the effective moment (M_{eff}), and the saturation moment (M_{sat} , the value measured at $T = 5$ K and $H = 500$ Oe) for $\text{Li}_{1+y}(\text{Zn}_{1-x}\text{Mn}_x)\text{P}$.

	y (excess Li)	T_C (K)	θ (K)	M_{sat} (μ_B/Mn)	M_{eff} (μ_B/Mn)	Coercivity (Oe)
$\text{Li}_{1+y}(\text{Zn}_{0.93}\text{Mn}_{0.07})\text{P}$	0.07	25	24.5	0.61	3.40	20
	0.10	24	23.0	0.32	2.40	16
	0.15	24	23.0	0.37	2.02	25
$\text{Li}_{1+y}(\text{Zn}_{0.9}\text{Mn}_{0.1})\text{P}$	0.07	22	19.8	0.19	1.94	24
	0.10	25	23.4	0.41	2.52	14
	0.12	22	18.4	0.23	2.34	20
	0.15	22	17.7	0.22	2.29	20

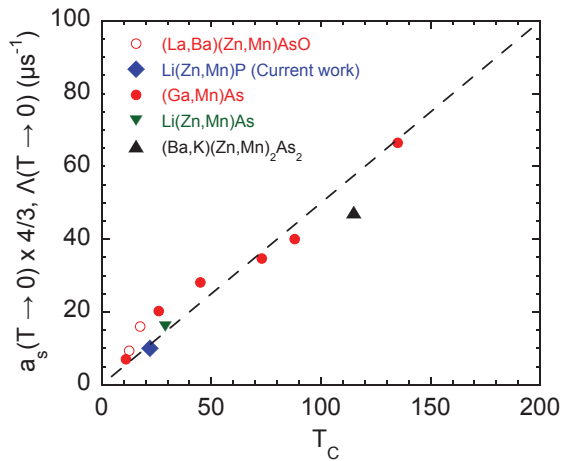


FIG. 5: (Color online) Correlation between the static internal field parameter a_s determined at 2 K by zero-field μSR versus Curie temperature T_C observed in $(\text{Ga},\text{Mn})\text{As}$ (Ref. 23), $\text{Li}(\text{Zn},\text{Mn})\text{As}$ (Ref. 13), $(\text{La},\text{Ba})(\text{Zn},\text{Mn})\text{AsO}$ (Ref. 16), $(\text{Ba},\text{K})(\text{Zn},\text{Mn})_2\text{As}_2$ (Ref. 20) and current work of $\text{Li}(\text{Zn},\text{Mn})\text{P}$. The nearly linear correlation indicates a common mechanism for the ferromagnetic exchange interaction; dashed line is a guide for the eye.

previously, the average internal magnetic field at the muon sites should be much larger than the applied field, and the oscillation amplitude is therefore an indicator of the paramagnetic volume.²⁷ WTF- μSR measurements provide direct information of the magnetic volume fraction.²⁷ Clearly, the amplitude of oscillation becomes smaller with decreasing T , indicating the suppression of the paramagnetic volume. We show the results of size of magnetically ordered volume derived from WTF- μSR in Fig. 4, and compare it with those derived from the measurements in ZF. Both are in good agreement, supporting the validity of our analysis of the ZF- μSR spectra using a two-component function. We note that the growth of ferromagnetic ordered volume below T_C in $\text{Li}(\text{Zn},\text{Mn})\text{P}$ is more gradual than previous reported $\text{Li}(\text{Zn},\text{Mn})\text{As}$ ¹³ and 122 type $(\text{Ba},\text{K})(\text{Zn},\text{Mn})_2\text{As}_2$,²⁰ this is primarily due to the distribution of T_C arising from sample synthesis. We have also conducted longitudinal-field μSR at 200 Oe

(not shown), and confirmed the relaxation observed in this material is due mostly to static magnetic field. The ordered volume fraction starts to grow below $\sim 22\text{K}$, indicating a ferromagnetic transition that takes place at $T_C \sim 22\text{K}$, which is consistent with the magnetization measurements. Magnetic volume fraction reaches up to nearly 100% at the base temperature of 2 K, implying that static magnetic order develops in almost the entire sample volume. This result is again consistent with the NMR observation that no NMR signals arising from magnetic impurities or Mn clusters are observed.²⁴ We believe that further improvement in fabrication and heating procedures will improve the homogeneity of ferromagnetism in this material.

We can extract the relaxation rate, a_s , from the fitting of ZF time spectra. a_s is proportional to the individual ordered moment size multiplied by the moment concentration. Similar to the case of $\text{Li}(\text{Zn},\text{Mn})\text{As}$,¹³ we plot a_s at the lowest measured temperature versus Curie temperature T_C in Fig. 5. A factor $4/3$ is multiplied to the parameter a_s for all bulk DFSs,^{13,16,20} to adjust the difference from the simple exponential decay rate adopted in $(\text{Ga},\text{Mn})\text{As}$.²³ a_s falls into the linear relation observed for $(\text{Ga},\text{Mn})\text{As}$ and other DFS families. The good agreement implies that all these DFS systems share a common mechanism for the ferromagnetic exchange interaction, including the current $\text{Li}(\text{Zn},\text{Mn})\text{P}$ system, despite its much lower carrier density.¹⁴

$\text{Li}_{1+y}(\text{Zn}_{1-x}\text{Mn}_x)\text{P}$ has the advantage of decoupled carrier and spin doping, where the Mn^{2+} substitution for Zn introduces spins and the Li^+ off-stoichiometry provides carriers. It has been shown that doping Mn^{2+} only in $\text{Li}_{1+y}(\text{Zn}_{1-x}\text{Mn}_x)\text{P}$, without excess lithium doping, will result in a paramagnetic ground state.¹⁴ Only with excess Li being doped, can ferromagnetic ordering develop. This enables us to investigate the influence of overdoped Li on the ferromagnetic state. In Fig. 6(a) and (b), we show dc magnetization and isothermal magnetization measured for $\text{Li}_{1+y}(\text{Zn}_{0.93}\text{Mn}_{0.07})\text{P}$ with a fixed Mn concentration of $x = 0.07$ and $y = 0.07, 0.10$ and 0.15 . We can see that all three specimens display strong ferromagnetic signals in both $M(T)$ and $M(H)$ curves. For example, $M(T)$ of $\text{Li}_{1.07}(\text{Zn}_{0.93}\text{Mn}_{0.07})\text{P}$ shows an strong enhancement below $T_C = 26$ K (T_C is extrapolated from

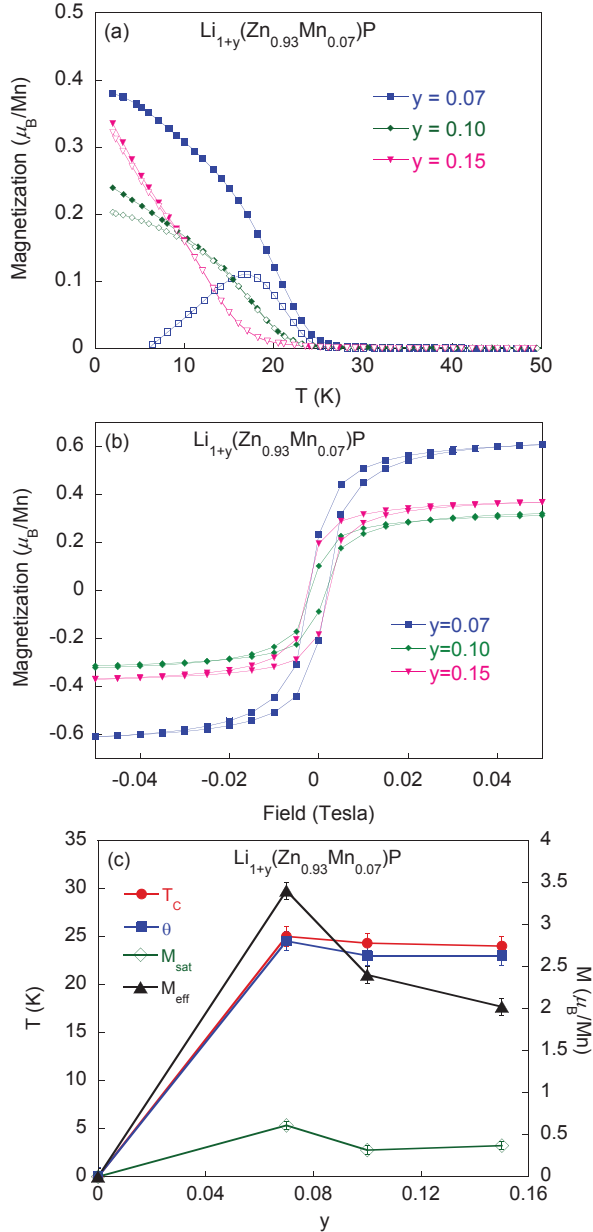


FIG. 6: (Color online) (a) dc magnetization for $\text{Li}_{1+y}(\text{Zn}_{0.93}\text{Mn}_{0.07})\text{P}$ ($y = 0.07, 0.10$ and 0.15) in both zero field cooling (ZFC, open symbols) and field cooling (FC, solid symbols) modes under $B_{ext} = 50$ Oe. (b) Isothermal magnetization measured at 5 K for $\text{Li}_{1+y}(\text{Zn}_{0.93}\text{Mn}_{0.07})\text{P}$ ($y = 0.07, 0.10$ and 0.15) specimens. (c) Curie temperature T_C , Weiss temperature θ , saturation moments M_{sat} and effective moments M_{eff} versus excess Li^+ concentrations y of $\text{Li}_{1+y}(\text{Zn}_{0.93}\text{Mn}_{0.07})\text{P}$.

$1/M \sim T$, see ref. 14), and $M(H)$ has a parallelogram shape with a coercive field of ~ 20 Oe. Another feature of the $\text{Li}_{1.07}(\text{Zn}_{0.93}\text{Mn}_{0.07})\text{P}$ specimen is that ZFC and FC curves display a bifurcation shortly below T_C . We fitted the $M(T)$ curve above T_C according to the Curie-Weiss law, $\chi - \chi_0 = C/(T - \theta)$, where C is Curie constant and θ

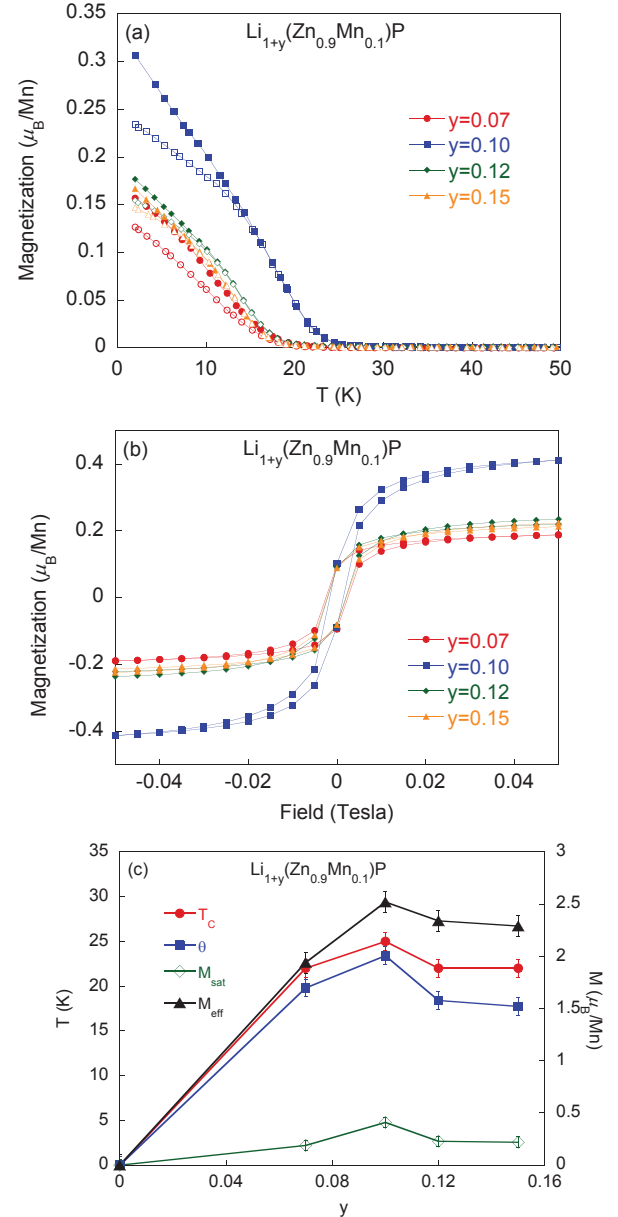


FIG. 7: (Color online) (a) dc magnetization for $\text{Li}_{1+y}(\text{Zn}_{0.9}\text{Mn}_{0.1})\text{P}$ ($y = 0.07, 0.10, 0.12$, and 0.15) in both ZFC (open symbols) and FC (solid symbols) modes under $B_{ext} = 50$ Oe. (b) Isothermal magnetization curves at 5 K. (c) T_C , θ , M_{sat} , and M_{eff} versus excess Li^+ concentrations y of $\text{Li}_{1+y}(\text{Zn}_{0.9}\text{Mn}_{0.1})\text{P}$.

the Weiss temperature, and derived the effective paramagnetic moment, M_{eff} , from the Curie constant C . M_{eff} is $\sim 3\mu_B/\text{Mn}$ for $y = 0.07$. This value is smaller than $4.5 \mu_B/\text{Mn}$ of $\text{Li}_{1.04}(\text{Zn}_{0.97}\text{Mn}_{0.03})\text{P}$ in ref. 14. $M_{eff} \sim 5-6 \mu_B/\text{Mn}$ is expected for high state Mn^{2+} ions. Apparently, the suppression of M_{eff} is not only arising from the competition of the antiferromagnetic exchange interaction of N.N. Mn^{2+} , but also from the overdoped carriers, as will be shown in detail in the following.

We plot Curie temperature (T_C), Weiss temperature (θ), the effective moment (M_{eff}), and the saturation moment (M_{sat} , the value measured at $T = 5$ K and $H = 500$ Oe) versus the nominal excess Li concentration in Fig. 6(c). For Li concentration equal to 1 (i.e., $y = 0$), $\text{Li}(\text{Zn}_{0.93}\text{Mn}_{0.07})\text{P}$ remains a paramagnetic ground state. We therefore define T_C , θ , M_{eff} and M_{sat} as zero, and plot zero in Fig. 6(c) for comparison. Clearly, we can see that all four parameters display qualitatively similar Li concentration dependence. They increase with Li concentration initially, reach a maximum at $y = 0.07$, and then start to decrease when overdoped with Li. To examine if the same trend is valid in a different Mn concentration, we also investigate these parameters in $\text{Li}_{1+y}(\text{Zn}_{0.9}\text{Mn}_{0.1})\text{P}$ (with $x = 0.10$ and $y = 0.07, 0.10, 0.12$ and 0.15), and show the results in Fig. 7. The situation is similar to the case of the $x = 0.07$ specimens. T_C , θ , M_{sat} , and M_{eff} first increase from $y = 0$ to $y = 0.07$, reach a maximum at $y = 0.10$, and then decrease from $y = 0.10$ to $y = 0.15$ for $\text{Li}_{1+y}(\text{Zn}_{0.9}\text{Mn}_{0.1})\text{P}$. We tabulate all these parameters in Table 1.

It has been theoretically proposed that in diluted magnetic semiconductors, spins are mediated by hole carriers through RKKY interaction.⁹ From NMR measurements²⁴ of $\text{Li}_{1.15}(\text{Zn}_{0.9}\text{Mn}_{0.1})\text{P}$, it has been shown that the spin lattice relaxation rate $\frac{1}{T_1}$ of Li(0) sites, where zero means no Mn at N.N. Zn sites for Li, display a Korringa behavior, i.e., Fermi surface excitations of a small number of conduction carriers. The $\frac{1}{T_1}$ of Li(Mn) site shows a T-independent behavior caused by spin fluctuations, i.e., representing local moments. This provides direct and convincing experimental evidence that Fermi degenerate conduction carriers mediate the Mn-Mn spin interactions through the p-d exchange interaction, and that the Mn-Mn spin interaction is long-ranged, rather than a nearest-neighbor exchange interactions.²⁴ The RKKY exchange interaction can be written as, $J \sim \cos(2k_F r)/r^3$, where k_F is the radius of Fermi surface (assuming the Fermi surface is a spherical shape) and r the distance between two localized moments. The first oscillation period of the RKKY

interaction supports ferromagnetic coupling. In our case, doping more Li introduces more carrier, and subsequently modifies the density of states and, therefore, the shape of Fermi surface. The modified Fermi surface affects the period of oscillation, as well as the ferromagnetic ordering.

IV. CONCLUSION

We conducted μSR investigation of a bulk form I-II-V DFS $\text{Li}_{1+y}(\text{Zn}_{1-x}\text{Mn}_x)\text{P}$. Our μSR results confirm the development of ferromagnetic ordering below T_C with a nearly 100% magnetically ordered volume. Despite its much lower carrier density, $\text{Li}_{1+y}(\text{Zn}_{1-x}\text{Mn}_x)\text{P}$ shares a common mechanism for the ferromagnetic exchange interaction with (Ga,Mn)As, Li(Zn,Mn)As, 1111 type (La,Ba)(Zn,Mn)AsO and 122 type (Ba,K)(Zn,Mn)₂As₂. Taking advantage of the decoupled nature of the carrier and spin doping in $\text{Li}_{1+y}(\text{Zn}_{1-x}\text{Mn}_x)\text{P}$, we investigated, for the first time, the influence of overdoped carriers on the ferromagnetic ordered state of a DFS. We found that overdoped Li suppresses both T_C and magnetic moments. A simple explanation is the modification of the Fermi surface caused by extra carriers. More detailed theoretical models are expected to explain this phenomena.

Acknowledgments

The work at Zhejiang was supported by National Basic Research Program of China (No. 2014CB921203, 2011CBA00103), NSF of China (No. 11274268); at IOP in Beijing by the NSFC and MOST; at Columbia by the U.S. NSF PIRE (Partnership for International Research and Education, Grant No. OISE-0968226) and Grant No. DMR-1105961; the JAEA Reimei Project at IOP, Columbia, PSI, and McMaster; and NSERC and CIFAR at McMaster. F.L. Ning acknowledges helpful discussions with I. Mazin, I. Zutic.

* Electronic address: ningfl@zju.edu.cn

¹ Munekata H., Ohno H., Molnar S. von, Segmüller Armin, Chang L. L., and Esaki L., (1989) Phys. Rev. Lett **63**, 1849.

² Ohno H., Shen A., Matsukura F., Oiwa A., Endo A., Katsumoto S., and Iye Y., (1996) Appl. Phys. Lett **69**, 363.

³ Samarth N., (2010) Nat. Mater. **9**, 955.

⁴ Chambers S., (2010) Nat. Mater. **9**, 956.

⁵ Dietl T., (2010) Nat. Mater. **9**, 965.

⁶ Dietl T., and Ohno H., (2014) Rev. Mod. Phys. **86**, 187.

⁷ Zutic I., Fabian J., and Das Sarma S., (2004) Rev. Mod. Phys. **76**, 323.

⁸ Jungwirth T., Sinova J., Masek J., Kucera J., and MacDonald A.H., (2006) Rev. Mod. Phys. **78**, 809.

⁹ Dietl T., Ohno H., Matsukura F., Cibert J., and Ferrand D., (2000) Science **287**,1019.

¹⁰ Wang M., Champion R. P., Rushforth A. W., Edmonds K. W., Foxon K. W., and Gallagher B. L., (2008) Appl. Phys. Lett. **93**, 132103.

¹¹ Chen L., Yan S., Xu P. F., Wang W. Z., Deng J. J., Qian X., Ji Y., and Zhao J. H., (2009) Appl. Phys. Lett. **95**, 182505.

¹² Chen L., Yang X., Yang F. H., Zhao J. H., Misuraca J., Xiong P., and Molnar S. V., (2011) Nano Lett. **11**, 2584.

¹³ Deng Z., Jin C. Q., Liu Q. Q., Wang X. C., Zhu J. L., Feng S. M., Chen L. C., Yu R. C., Arguello C., Goko T., Ning F. L., Zhang J. S., Wang Y. Y., Aczel A. A., Munsie T., Williams T. J., Luke G. M., Kakeshita T., Uchida S.,

- Higemoto W., Ito T. U., Gu B., Maekawa S., Morris G. D. and Uemura Y. J., (2011) *Nat. Commun.* **2**, 422.
- ¹⁴ Deng Z., Zhao K., Gu B., Han W., Zhu J. L., Wang X. C., Li X., Liu Q. Q., Yu R. C., Goko T., Frandsen B., Liu L., Zhang J. S., Wang Y. Y., Ning F. L., Maekawa S., Uemura Y. J., and Jin C. Q., (2013) *Phys. Rev. B* **88**, 081203(R).
- ¹⁵ Wang Q., Man H. Y., Ding C., Gong X., Guo S. L., Wang H. D., Chen B., and Ning F. L., (2014) *J. Appl. Phys.* **115**, 083917.
- ¹⁶ Ding C., Man H. Y., Qin C., Lu J. C., Sun Y. L., Wang Q., Yu B. Q., Feng C. M., Goko T., Arguello C. J., Liu L., Frandsen B. A., Uemura Y. J., Wang H. D., Luetkens H., Morenzoni E., Han W., Jin C. Q., Munsie T., Williams T. J., D'Ortenzio R. M., Medina T., Luke G. M., Imai T., and Ning F. L., (2013) *Phys. Rev. B* **88**, 041102(R).
- ¹⁷ Lu J. C., Man H. Y., Ding C., Wang Q., Yu B. Q., Guo S. L., Wang H. D., Chen B., Han W., Jin C. Q., Uemura Y. J., and Ning F. L., (2013) *Europhys. Lett.* **103**, 67011.
- ¹⁸ Yang X. J., Li Y. K., Shen C. Y., Si B. Q., Sun Y. L., Tao Q., Cao G. H., Xu Z. A., and Zhang F. C., (2013) *Appl. Phys. Lett.* **103**, 022410.
- ¹⁹ Han W., Zhao K., Wang X. C., Liu Q. Q., Ning F. L., Deng Z., Liu Y., Zhu J. L., Ding C., Man H. Y., and Jin C. Q., (2013) *Sci. China-Phys. Mech. Astron.* **56**, 2026.
- ²⁰ Zhao K., Deng Z., Wang X. C., Han W., Zhu J. L., Li X., Liu Q. Q., Yu R. C., Goko T., Frandsen B., Liu L., Ning F. L., Uemura Y. J., Dabkowska H., Luke G. M., Luetkens H., Morenzoni E., Dunsiger S. R., Senyshyn A., Böni P., and Jin C. Q., (2013) *Nat. Commun.* **4**, 1442.
- ²¹ Yang X. J., Li Y. K., Zhang P., Luo Y. K., Chen Q., Feng C. M., Cao C., Dai J. H., Tao Q., Cao G. H., and Xu Z. A., (2013) *J. Appl. Phys.* **114**, 223905.
- ²² Man H. Y., Qin C., Ding C., Wang Q., Gong X., Guo S. L., Wang H. D., Chen B., and Ning F. L., (2014) *Europhys. Lett.* **105**, 67004.
- ²³ Dunsiger S. R., Carlo J. P., Goko T., Nieuwenhuys G., Prokscha T., Suter A., Morenzoni E., Chiba D., Nishitani Y., Tanikawa T., Matsukura F., Ohno H., Ohe J., Maekawa S., and Uemura Y. J., (2010) *Nat. Mater.* **9**, 299.
- ²⁴ Ding C., Qin C., Man H. Y., Imai T., and Ning F. L., (2013) *Phys. Rev. B* **88**, 041108(R).
- ²⁵ Kuriyama K., Katoh T., and Mineo N., (1991) *J. Cryst. Growth* **108**, 37.
- ²⁶ Bacewicz R., and Cizek T. F., (1988) *Appl. Phys. Lett.* **52**, 1150.
- ²⁷ Uemura Y. J., Goko T., Gat-Malureanu I. M., Carlo J. P., Russo P. L., Savici A. T., Aczel A., MacDougall G. J., Rodriguez J. A., Luke G. M., Dunsiger S. R., McCollam A., Arai J., Pfeleiderer Ch., Böni P., Yoshimura K., Baggio-Saitovitch E., Fontes M. B., Larrea J., Sushko Y. V., and Sereni J., (2007) *Nat. Phys.* **3**, 29.